第 34 卷第 8 期
2018 年 8 月

无 机 化 学 学 报
CHINESE JOURNAL OF INORGANIC CHEMISTRY

Vol.34 No.8
1538-1546

2,4-二羟基苯甲酸辅助合成不同形貌二氧化铈及其在 NH_3-SCR 中的应用

苏 航 徐 蔓 周诗健 杨 福 孔 岩*

(南京工业大学化工学院,材料化学工程国家重点实验室,南京 210009)

摘要：使用 2,4-二羟基苯甲酸(DHBA)辅助控制合成出具有不同形貌(棒状与片状)的碱式碳酸铈。在水热阶段,碱式碳酸铈的形貌可以通过 DHBA 的量进行调控。当 DHBA 为 3.5 mmol 时,得到棒状碱式碳酸铈,然而增加 DHBA 的量至 5.0 mmol 时,可形成片状碱式碳酸铈。棒状与片状 *fcc*-CeO_2(面心立方二氧化铈)可成功地通过相应的焙烧处理获得。所得二氧化铈均有较大的比表面积(>60 $m^2 \cdot g^{-1}$),然而与片状二氧化铈相比,棒状二氧化铈有更高的氧化还原能力与更多的酸量。棒状二氧化铈用于 NH_3-SCR 时有着更好的催化活性。

关键词：二氧化铈；2,4-二羟基苯甲酸；纳米结构；水热合成；NH_3-SCR

中图分类号：O643.36；TB34　　**文献标识码**：A　　**文章编号**：1001-4861(2018)08-1538-09

DOI:10.11862/CJIC.2018.168

CeO_2 in Different Morphologies with 2,4-Dihydroxybenzonic Acid as Auxiliary: Synthesis and Application in NH_3-SCR

SU Hang　XU Man　ZHOU Shi-Jian　YANG Fu　KONG Yan*

(*State Key Laboratory of Materials-Oriented Chemical Engineering, College of Chemical Engineering, Nanjing Tech University, Nanjing* 210009, *China*)

Abstract: Different morphologies (rod-like and sheet-like) of $CeOHCO_3$ were controllably synthesized by using 2,4-dihydroxybenzonic acid (DHBA) as auxiliary. During the hydrothermal process, the morphologies of $CeOHCO_3$ were controlled by adding different amount of DHBA. When the amount of DHBA was 3.5 mmol, rod-like $CeOHCO_3$ was synthesized, while by increasing the amount of DHBA to 5.0 mmol, the sheet-like $CeOHCO_3$ was relatively generated. Then the rod-like and sheet-like *fcc*-CeO_2 (face-centered cubic-CeO_2) were successfully obtained by the subsequent calcination procedure. The resulted CeO_2 affords large surface area (> 60 $m^2 \cdot g^{-1}$), while the rod-like CeO_2 exhibits higher redox ability and more acid amount compared to those of sheet-like CeO_2. In addition, the rod-like CeO_2 exhibits better catalytic activity in NH_3-SCR.

Keywords: CeO_2; 2,4-dihydroxybenzonic acid; nanostructure; hydrothermal synthesis; NH_3-SCR

0 Introduction

In recent decades, metal oxides have been intensely applied in the fields of catalysis[1-2], sensor[3-4], lithium-ion battery[5-6], *etc*. Particularly, metal oxides with controlled shapes have positive effect in heterogeneous catalysis system. Some related properties, such as the specific architecture and high surface area

收稿日期:2018-03-07。收修改稿日期:2018-05-03。

国家自然科学基金(No.21476108,21476108,21476108,21706121),江苏省自然科学基金(No.BK20170995),江苏省高校自然科学研究项目(No.16KJB530003)和江苏省高等教育机构重点学科建设项目(PAPD)资助。

*通信联系人。E-mail:kongy36@njtech.edu.cn

have important influence on the anchoring of the active sites and controlling the diffusion of reactants. With the well-defined morphologies, the researchers can not only adjust the required physicochemical properties but also improve the catalytic performance[7]. Therefore, it is of great significance to explore facile and controllable routes for designing the desired structures.

As well known, nitrogen oxides remain the major pollution source in the air, which could result in the formation of photochemical smog, ozone depletion and acid rain[8]. These situations are directly harmful to ecological environment and human health. In order to address this dilemma, some effective approaches are expected. Fortunately, selective catalytic reduction of NO with NH_3 has been regarded as one of the considerable technologies for the abatement of NO (NH_3-SCR), and the process can be described by the following equation:

$$4NO+4NH_3+O_2 \rightarrow 4N_2+6H_2O$$

Besides, as one of the metal oxides, ceria (CeO_2) has been continually focused owing to the highly oxygen storage capacity, enhanced metal dispersion and facile stabilization of the support[9-10]. Meantime, CeO_2 can also serve as an outstanding component in the field of selective catalytic reduction of NO with NH_3[11]. However, the CeO_2-based materials have been significantly demonstrated that the morphologies are closely associated with the physicochemical properties. Typically, for the pure CeO_2, hollow ceria nanosphere with multiple shells exhibited distinguishable photocatalytic activity in water oxidation[12]. With regard to the hybrid CeO_2-based materials, core-shell Pd@CeO_2 nanostructures were found to exhibit excellent catalytic activity in NO reduction[13]. Recently, in the system of NH_3-SCR, Li et al. reported that the novel MnO_x-CeO_2 nanosphere showed superior activity than the non-structured MnO_x-CeO_2 catalyst[14]. Hybrid multi-shell hollow structured CeO_2-MnO_x was designed and found that this material displayed excellent catalytic activity compared to the traditional CeO_2-MnO_x nanoparticles or single-shell hollow spheres[15]. Although great efforts have been achieved, there is still room for controllable synthesis of CeO_2 with specific morphologies and apply to NH_3-SCR.

To control the morphology of CeO_2, some efficient methods, such as hydrothermal[16], polyol method[17], template method[18] and colloidal solution combustion[19] have been adopted. While, in consideration of the tunable reaction parameters, such as different temperatures and additives, the hydrothermal method could be considered as a promising route. Notably, benzoic acid compounds have been achieved to prepare various polymers, pharmaceuticals and metal-organic framework particles (MOFs). Especially, Fan et al.[20] reported $CuFe_2O_4$@HKUST-1 heterostructures with MOFs shell were constructed by 1,3,5-benzenetricarboxylic acid. Korpany et al.[21] explored a series of benzoic acid derivatives to fabricate surface functionalized iron oxide nanoparticles. Plentiful functional materials have opened a door to discover the relationship between benzoic acid derivatives and nanomaterials. Therefore, choosing the appropriate method as well as the suitable benzoic acid compounds play an important role in the synthesis of desirable nanoparticles. Whereas, to the best of our knowledge, it is still lack the research in controlling synthesis of nanocrystallines including CeO_2 by using benzoic acid derivatives.

Herein, the rod-like and sheet-like CeO_2 were successfully synthesized with the assistant of 2,4-dihydroxybenzonic acid. The selected 2,4-dihydroxybenzonic acid could be completely dissolved in the reaction system to form a homogeneous solution. Time-dependent and temperature-dependent experiments were carried out to study the growth mechanism of the CeO_2. Besides, the physicochemical properties of the CeO_2 were investigated. In addition, the catalytic activity of the as-prepared CeO_2 was evaluated in the system of NH_3-SCR.

1　Experimental

The rod-like CeO_2 was synthesized via the hydrothermal method and the calcination procedure. Typically, 2 mmol of $Ce(NO_3)_3 \cdot 6H_2O$ and 3.5 mmol of 2,4-dihydroxybenzoic acid (DHBA) were dissolved in

the mixed solution of 15.0 mL ethanol and 30.0 mL deionized water. Then 5.0 mL of sodium acetate solution (0.5 mol·L^{-1}) was added dropwise into the mixed solution with stirring. The obtained homogeneous solution was transferred into a Teflon-lined autoclave and heated at 180 ℃ for 24 h in an electric oven. Moreover, the autoclave was cooled to room temperature, the precipitate was centrifuged and washed with deionized water for four times and dried at 60 ℃ for 6 h. Then the precursor (Ce-Pre-1) was calcined in air atmosphere at 500 ℃ with a heat ramp rate of 2 ℃·min^{-1} for 4 h, and the calcined products were named as Ce-Cal-1.

Instead, the sheet-like CeO_2 was obtained according to the similar process of rod-like CeO_2 by increasing the amount of DHBA to 5 mmol, and the hydrothermal products and the calcined products were labeled as Ce-Pre-2 and Ce-Cal-2, respectively.

Time-dependent experiments for the precursors of Ce-Cal-1 and Ce-Cal-2 were carried out at different hydrothermal intervals of 3, 6, 10 and 21 h without changing other reaction parameters. The temperature-dependent experiments of Ce-Cal-2 were performed at 120, 140 and 160 ℃, respectively.

X-ray diffraction patterns (XRD) was used for characterizing the phase purity with a monochromatic Cu $K\alpha$ radiation source (λ =0.154 178 nm) and operated at 40 kV and 100 mA in the range of 10°~80°. Field-emission scanning electron microscopy (FE-SEM) was performed on a Hitachi S4800 Field-Emission Scanning Electron Microscope and operated at 5 kV. High-resolution transmission electron microscopy (HRTEM) images were recorded on an EM-2010 EX microscope with the accelerating voltage at 200 kV. The N_2 adsorption-desorption isotherms were carried out in the relative pressure (P/P_0) range from 0.01 to 0.99, and the surface area of samples were calculated by Brunauer-Emmet-Teller equation (BET). Temperature-programmed reduction under H_2 environment (H_2-TPR) was carried out on a TP-5000 instrument. 50 mg CeO_2 was pretreated under He-O_2 stream at 500 ℃ for 1 h. After cooling down to room temperature, the catalyst was purged with 30 mL·min^{-1} of He for 30 min to remove the excess O_2. Then the flow of 5% H_2-He was introduced into the sample with a flow rate of 30 mL·min^{-1} and the temperature was raised to 950 ℃ at a rate of 10 ℃·min^{-1}. The acidity of the CeO_2 was measured by NH_3 temperature programmed desorption (NH_3-TPD) in the same instrument as the H_2-TPR. Prior to TPD experiment, 100 mg CeO_2 was pretreated at 300 ℃ for 30 min and cooling to 50 ℃ under argon flow. The sample was exposed to a flow of 2.500 g·L^{-1} NH_3/Ar (50 mL·min^{-1}) at 100 ℃ for 1 h, followed by argon purging for another 1 h. Then, the temperature was raised to 950 ℃ in argon flow at the rate of 10 ℃·min^{-1}. Thermogravimetry and differential scanning calorimetry (TG-DSC) was measured by a NETZSCH STA 409 instrument with a heating rate of 10 ℃·min^{-1} under nitrogen atmosphere. Fourier transform infrared (FT-IR) spectra of the samples were obtained in the range of 4 000~500 cm^{-1} with powders dispersed in KBr on Bruker VECTOR22 resolution.

The catalytic conversion of NO was measured via a fixed-bed reactor with 0.2 g pure CeO_2 (40~60 mesh) as catalyst. The feed gas contained 500 mg·L^{-1} NH_3, 500 mg·L^{-1} NO, 5% (V/V) O_2, 5% (V/V) H_2O, with N_2 as the balance gas. The total flow rate of the feed gas was 200 mL·min^{-1}, corresponding to a space velocity of 60 L·g^{-1}·h^{-1}. The concentration of NO was detected by an onlin e Thermo fisher IS10 FTIR spectrometer equipped with a 2 m path-length gas cell (250 mL). The NO conversion can be calculated by NO conversion=$(c_{NO,in}-c_{NO,out})/c_{NO,in}\times 100\%$.

2 Results and discussion

Fig.1(a) and Fig.1(e) show the X-ray diffraction patterns (XRD) of Ce-Cal-1 and Ce-Cal-2. The diffraction peaks at *ca.* 28.5°, 32.9°, 47.3°, 56.2°, 59.1°, 69.4°, 76.5°, 78.7° are well indexed to the face-centered cubic CeO_2 (*fcc*-CeO_2, PDF No.34-0394), implying the samples are not amorphous. Fig.1 (b) depicts the typical rod-morphology of Ce-Cal-1 with the average width of 100~300 nm and the average length of 500 nm~1.5 μm. The TEM image in Fig.1(c) also reveals the rod-like profile of CeO_2. Fig.1 (d)

presents the corresponding HRTEM image of Ce-Cal-1. As shown in Fig.1 (d), the lattice fringe spacing of 0.27 and 0.31 nm correspond to (200) and (111) diffraction planes of CeO_2, respectively. On the other hand, Ce-Cal-2 displays the sheet morphology with the thickness below 80 nm and the length can reach to 700 nm (Fig.1(f) and Fig.1(g)). The obvious lattice fringe spacing of 0.31 nm in Fig.1(h) matches well with (111) diffraction plane of CeO_2. In addition, the SAED profiles manifest the typical single crystal, and some defects of the resulted CeO_2 could be discovered (marked as green rectangles). Therefore, the rod-like and sheet-like CeO_2 are successfully synthesized in this case.

The N_2 adsorption-desorption isotherms of CeO_2 were measured and shown in Fig.2 (a) and Fig.2(b). The BET surface areas of the Ce-Cal-1 and Ce-Cal-2 are calculated as about 61 $m^2 \cdot g^{-1}$ and 68 $m^2 \cdot g^{-1}$,

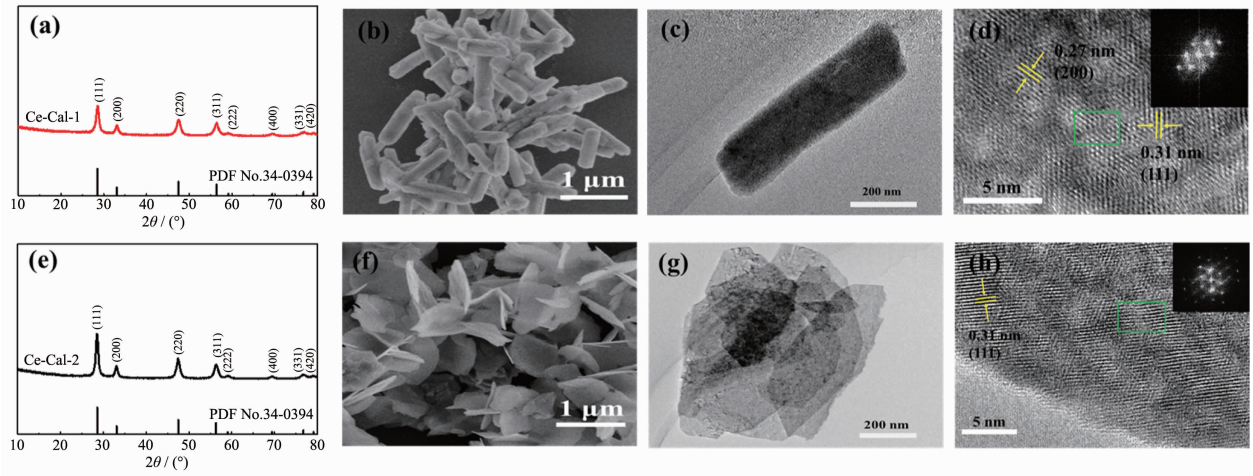

Fig.1　XRD patterns (a, e), SEM images (b, f), TEM images (c, g), HRTEM images (d, h) with the corresponding SAED (inset) of Ce-Cal-1 and Ce-Cal-2, respectively

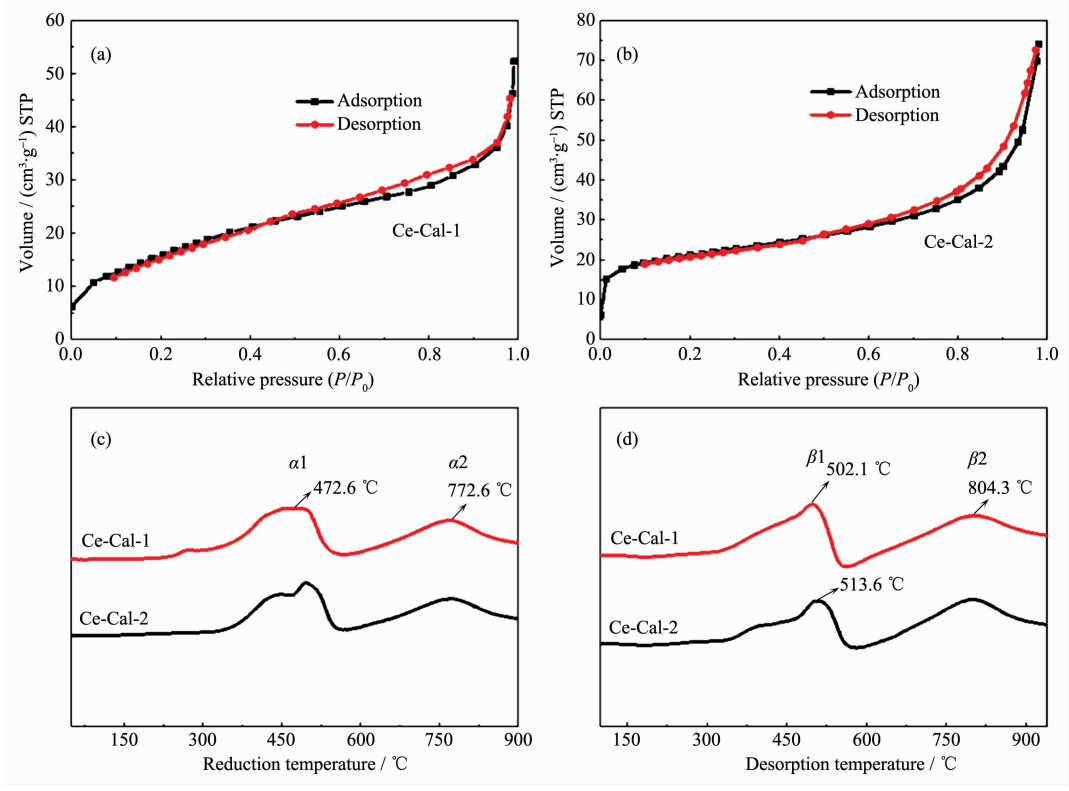

Fig.2　N_2 adsorption-desorption isotherms (a, b), H_2-TPR (c) and NH_3-TPD profiles (d) of Ce-Cal-1 and Ce-Cal-2

respectively. Temperature-programmed reduction under H_2 environment (H_2-TPR) was tested to detect the redox property of the resulted CeO_2 (Fig.2(c)). Both the samples manifest the similar reduction peak positions, which are in good agreement with the pure ceria in other reports[22-23]. To be specific, the $\alpha1$ peak at the lower temperature between 250 ~600 ℃ could be attributed to the reduction of the absorbed surface oxygen species and the surface oxygen species of CeO_2. The $\alpha2$ peak in the range of 750~800 ℃ could be ascribed to the reduction of bulk oxygen. The H_2 consumption amount of Ce-Cal-1 at $\alpha1$ is higher than that of Ce-Cal-2, which could be attributable to the abundant surface oxygen species in Ce-Cal-1 (Table 1). Meantime, some differences of the bulk oxygen are also presented ($\alpha2$), which may be connected with the different structures. Temperature-programmed desorption experiments of NH_3 (NH_3-TPD) were examined to understand the acidity strength, and the results are presented in Fig.2(d). The desorbed $\beta1$ peak presents at the lower temperature of 300~570 ℃, corresponding to the desorption of physisorbed NH_3 and NH_3 at the weak acid sites[24]. While the desorbed $\beta2$ peak ranging between 570 and 940 ℃ is assigned to NH_3 absorbed at the strong acid sites[25]. The desorbed peak positions of the acid sites are analogous with each other; however, the NH_3 amount of $\beta1$ and $\beta2$ in Ce-Cal-1 are higher than those in Ce-Cal-2, indicating that the Ce-Cal-1 could possess of more acid sites. Moreover, the acid amount of the strong acid sites in both Ce-Cal-1 and Ce-Cal-2 are higher than those in the weak acid sites. Therefore, the H_2 consumption and NH_3 desorption amount of Ce-Cal-1 are higher than those of Ce-Cal-2, possibly associating with the diverse shapes and different exposed crystalline facets[26-27]. Distinguishable physicochemical properties of the as-prepared rod-like and sheet-like CeO_2 can be discovered.

To reveal the crystal phase and morphology evolution for the precursors of Ce-Cal-1 and Ce-Cal-2, time-dependent experiments were investigated. As displayed for the precursors of Ce-Cal-1 (Fig.3(a)), the diffraction peaks of the samples can be well indexed to pure orthorhombic phase of $CeOHCO_3$ (PDF No.41-0013). However, with regard to the precursors of Ce-Cal-2 (Fig.3(b)), the resulted precursors show the gradual phase transformation behaviors from orthorhombic phase (initial period) to hexagonal phase (final period). As expected, those products can be completely transformed into hexagonal phase of $CeOHCO_3$ (PDF No.32-0189) with the longer reaction time (21 and 24 h). It is noticeable that the mixed phases of orthorhombic and hexagonal are involved in the intermediate stages.

Besides, representative SEM images of the precursors at different reaction intervals were examined. For the precursors of Ce-Cal-1, the SEM images display the simplex rod-like morphology from Fig.3(c) to Fig.3(g) without obvious morphology transformation. However, as depicted from Fig.3(h) to Fig.3(l), the product affords rod-like structure at initial 3 h, and then the rod particles partially dissolve and accompany with the presence of some apparently granular particles (6 and 10 h). Finally, more sheet-like particles emerge as the dominant state (21 and 24 h). It should be noted that when the reaction system is absence of DHBA, the hydrothermal product presents the pure phase of CeO_2 with irregular morphology (Fig.4). Those results indicate that the $CeOHCO_3$ with specific morphology fails to be obtained in this condition.

Table 1 Quantitative analysis of H_2-TPR and NH_3-TPD

Catalyst	H_2-TPR			NH_3-TPD		
	H_2 consumption / a.u.[a]			NH_3 amount / a.u.[b]		
	$\alpha1$	$\alpha2$	$\alpha1+\alpha2$	$\beta1$	$\beta2$	$\beta1+\beta2$
Ce-Cal-1	1 090	946	2 036	8 187	9 385	17 572
Ce-Cal-2	849	864	1 713	5 999	7 941	13 940

[a,b] H_2 consumption and NH_3 amount are calculated from the corresponding peak area, respectively.

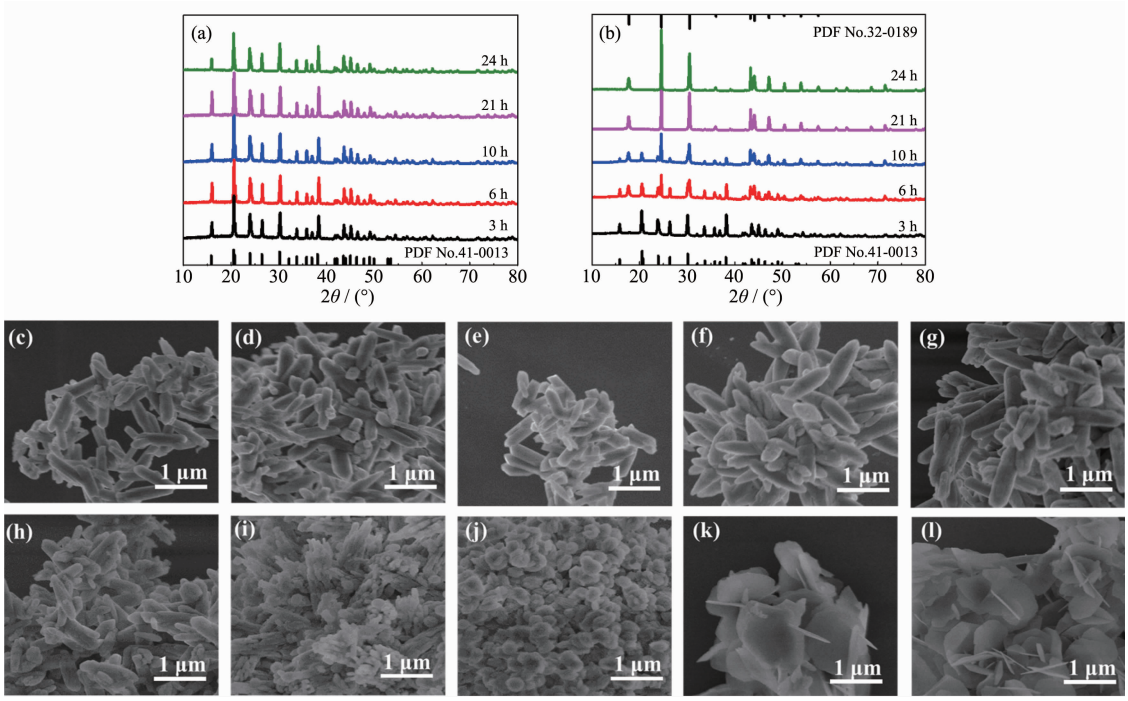

Fig.3　XRD patterns of the precursors Ce-Cal-1 (a) and Ce-Cal-2(b) at different hydrothermal intervals; SEM images for the precursors of Ce-Cal-1 (c~g) and Ce-Cal-2 (h~l) at different reaction intervals of 3, 6, 10, 21 and 24 h, respectively

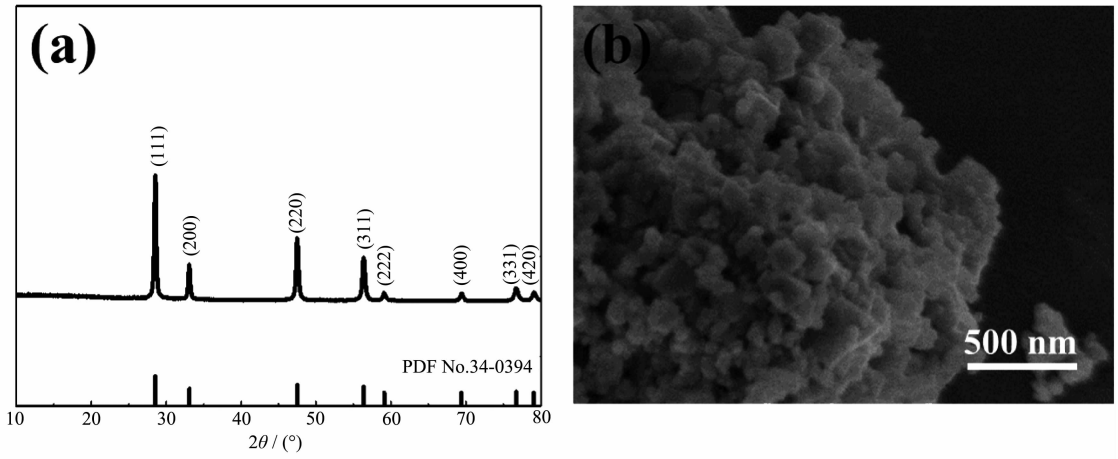

Fig.4　XRD pattern(a) and SEM image(b) of the hydrothermal product synthesized without DHBA

Temperature-dependent experiments based on Ce-Cal-2 were carried out and the SEM images are shown in Fig.5. The sample obtained at 120 ℃ exhibits the rod-like structure with the average width of 300~500 nm and the length below 3 μm. Moreover, those particles present the highly decentralized state without significant aggregation. However, as the temperature up to 140 and 160 ℃, the products exhibit the rod-like morphology with the state of aggregation. Obviously, the typical sheet-like morphology of the product can be observed as the temperature reaching to 180 ℃ (Ce-Pre-2). This phenomenon indicates that a morphology reconstruction process could be triggered with the high temperature.

For investigating the inorganic species of Ce-Pre-1 and Ce-Pre-2, FT-IR was recorded and the results are displayed in Fig.6(a). The Ce-Pre-1 is taken as an example to illustrate. The peak at *ca.* 3 461 cm^{-1} could be due to the stretching vibration of O-H groups in the adsorbed water, and the bending mode of O-H at *ca.* 1 638 cm^{-1} could also be observed. The band at *ca.* 1 561 cm^{-1} should be attributable to the asymmetric

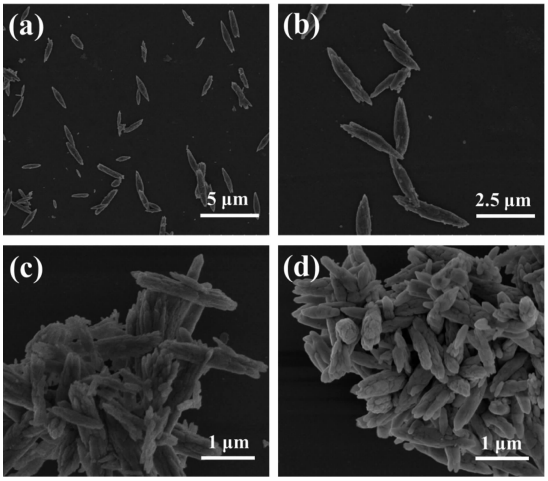

Fig.5 SEM images of the hydrothermal products at 120 ℃ (a, b), 140 ℃ (c) and 160 ℃ (d)

stretching of CO_2. Another sharp peak at *ca.* 1 420 cm^{-1} may be assigned to the stretching vibration of CO_3^{2-}. Besides, in the region of 700~900 cm^{-1}, the bands at *ca.* 861 and *ca.* 724 cm^{-1} are correspondingly attributed to the deformation of CO_3^{2-} and asymmetric vibration of CO_2 species, respectively. The peak at ca. 594 cm^{-1} could be ascribed to the Ce-O stretching band[28]. Some of the characteristic peaks including the stretching vibration and bending mode of O-H, the asymmetric stretching of CO_2 and the stretching band of Ce-O in Ce-Pre-2 are similar to Ce-Pre-1, indicating the same component of the two samples ($CeOHCO_3$). However, some difference can be found in the range of 1 400~1 500 cm^{-1} and 700~900 cm^{-1}, which could be due to the different crystal phases and morphologies of the $CeOHCO_3$. In addition, the thermostability of Ce-Pre-1 and Ce-Pre-2 were analyzed by thermogravimetry and differential scanning calorimetry (TG-DSC). As can be seen from Fig.6(b) and Fig.6(c), the curves manifest the weight loss between 240 and 300 ℃ with the major exothermic peak. The weight loss of Ce-Pre-1 and Ce-Pre-2 are approximately 21.8% and 21.2%, respectively, which are close to the theoretical decomposition value of $CeOHCO_3$ to CeO_2 (20.7%).

Based on the above-mentioned characterization and analysis, we tentatively propose that the DHBA could decompose into carbon species (CO_3^{2-}). The OH^- could also be produced by the hydrolysis of CO_3^{2-}, CH_3COO^- under the hydrothermal condition. Thus, Ce^{3+} could combine with OH^- and CO_3^{2-} to generate small granules with high surface energy. Meantime, the sustaining nucleation could be favorable to the growth of rod-like orthorhombic phase of $CeOHCO_3$. It is noticeable that the rod-like $CeOHCO_3$ could exist as the stable product with 3.5 mmol of DHBA (Fig.7, Route 1). While the process of dissolution and

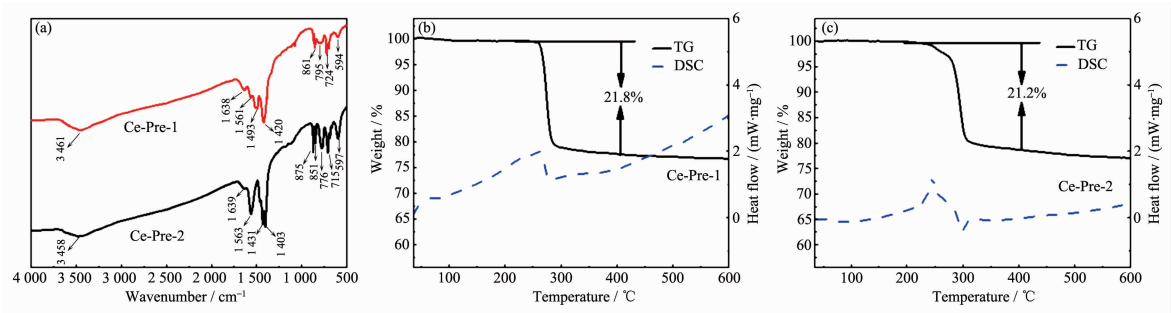

Fig.6 FT-IR spectra (a), TG-DSC curves (b, c) of Ce-Pre-1 and Ce-Pre-2

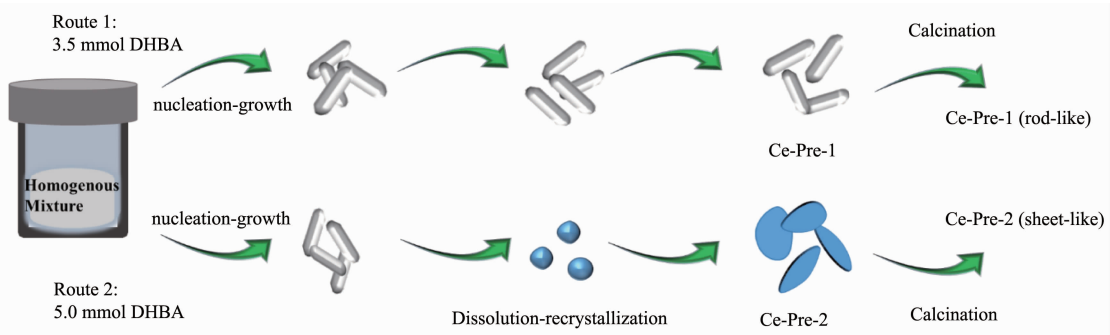

Fig.7 Illustration for the possible morphology evolution process for the Ce-Cal-1 and Ce-Cal-2

recrystallization could be triggered with 5.0 mmol of DHBA, and rod-like $CeOHCO_3$ could dissolve and reconstruct to form the sheet-like hexagonal phase of $CeOHCO_3$ ultimately (Fig.7, Route 2). As reported, the defects of the crystals could induce the dissolution and recrystallization process for the formation of CeO_2 with nanosheet morphologies[29-30]. However, in consideration of the different experiment conditions, the high content of the DHBA and high hydrothermal temperature could also play the important roles in this process. Furthermore, the as-prepared CeO_2 could preserve the rod-like and sheet-like morphologies after calcination.

In this work, Ce-Cal-1 and Ce-Cal-2 are used as catalysts for eliminating NO with NH_3. As shown in Fig.8, both of the samples present the similar trend of NO conversion from 100 to 400 ℃. With increasing the temperature to 350 ℃, Ce-Cal-1 shows the higher conversion about 69.2% compared with Ce-Cal-2 (50.9%). According to the results of H_2-TPR and NH_3-TPD, this phenomenon could be due to that Ce-Cal-1 possesses of the higher redox ability and more acid amount. The obtained CeO_2 particles exhibit structure-dependent catalytic activity for the catalytic reduction of NO. Besides, both the NO conversion of Ce-Cal-1 and Ce-Cal-2 are higher than the reported pure CeO_2, indicating high catalytic activity of Ce-Cal-1[31]. On the account of the catalytic results, the rod-like CeO_2 could be viewed as the optimized structure for the reaction.

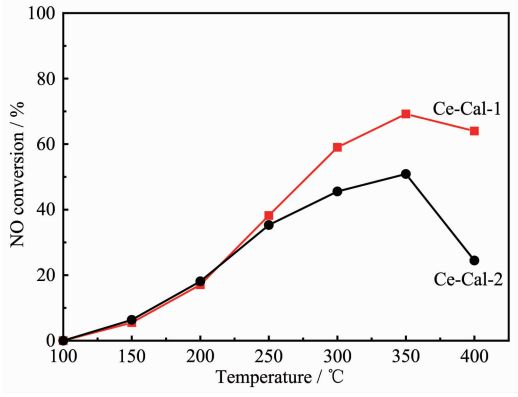

Fig.8　NO conversion of the Ce-Cal-1 and Ce-Cal-2

3　Conclusions

In summary, the rod-like and sheet-like $CeOHCO_3$ were successfully synthesized with the assistant of 2,4-dihydroxybenzonic acid. The rod-like orthorhombic phase of $CeOHCO_3$ was proposed as the stable product via the nucleation growth process, and the dissolution and recrystallization accompanied with the morphology evolution and phase transformation were supposed to the generation of sheet-like hexagonal phase of $CeOHCO_3$. The highly dispersed rod-like $CeOHCO_3$ could be obtained under the low hydrothermal temperature, while the state of aggregation and the transformation of morphology could be triggered by the high temperature. The obtained CeO_2 presented distinguishable structure-dependent properties, and the rod-like CeO_2 exhibited higher redox ability and more acid amount. Moreover, the rod-like CeO_2 manifested the better catalytic activity in NH_3-SCR. Furthermore, it is proposed that more benzoic acid compounds can be expected to fabricate metal oxides with desirable morphologies.

References:

[1] Mitsudome T, Yamamoto M, Maeno Z, et al. *J. Am. Chem. Soc.*, **2015**,**137**(42):13452-13455

[2] Yen H, Seo Y, Kaliaguine S, et al. *Angew. Chem. Int. Ed.*, **2012**,**51**(48):12032-12035

[3] Li Y, Luo W, Qin N, et al. *Angew. Chem. Int. Ed.*, **2014**,**53**(34):9035-9040

[4] PENG Juan(彭娟), LI Ye(李晔), JI Peng-Yu(季鹏宇), et al. *Chinese J. Inorg. Chem.*(无机化学学报), **2012**,**28**(6):1251-1258

[5] Bai J, Li X, Liu G, et al. *Adv. Funct. Mater.*, **2014**,**24**(20):3012-3020

[6] Cai D P, Wang D D, Huang H, et al. *J. Mater. Chem. A*, **2015**,**3**(21):11430-11436

[7] Florea I, Feral-Martin C, Majimel J, et al. *Cryst. Growth Des.*, **2013**,**13**(3):1110-1121

[8] Qi G S, Yang R T, Chang R. *Appl. Catal. B*: *Environ.*, **2004**, **51**(2):93-106

[9] Sayle D C, Maicaneanu S A, Watson G W. *J. Am. Chem. Soc.*, **2002**,**124**(38):11429-11439

[10]Premkumar T, Govindarajan S, Coles A E, et al. *J. Phys. Chem. B*, **2005**,**109**(13):6126-6129

[11]Tang C J, Zhang H L, Dong L. *Catal. Sci. Technol.*, **2016**,**6**(5):1248-1264

[12]Qi J, Zhao K, Li G, et al. *Nanoscale*, **2014**,**6**(8):4072-4077

[13]Wang X, Zhang Y, Song S, et al. *Angew. Chem. Int. Ed.*, **2016**,**55**(14):4542-4546

[14]Li L, Sun B, Sun J, et al. *Catal. Commun.*, **2017**,**100**:98-102

[15]Ma K, Zou W, Zhang L, et al. *RSC Adv.*, **2017**,**7**(10):5989-5999

[16]WEI Zhong-Bin(位忠斌), CUI Yu-Qian(崔育倩), GUO Pei-Zhi(郭培志), et al. *Chinese J. Inorg. Chem.*(无机化学学报), **2011**,**27**(7):1399-1404

[17]Ho C, Yu J C, Kwong T, et al. *Chem. Mater.*, **2005**,**17**(17):4514-4522

[18]YUE Lin(乐琳), ZHANG Xiao-Ming(张晓鸣). *Chinese J. Inorg. Chem.*(无机化学学报), **2008**,**24**(5):715-722

[19]Voskanyan A A, Chan K Y, Li C Y V. *Chem. Mater.*, **2016**, **28**(8):2768-2775

[20]Fan S, Dong W, Huang X, et al. *ACS Catal.*, **2017**,**7**(1):243-249

[21]Korpany K V, Majewski D D, Chiu C T, et al. *Langmuir*, **2017**,**33**(12):3000-3013

[22]Liu W, Feng L, Zhang C, et al. *J. Mater. Chem. A*, **2013**,**1**(23):6942-6948

[23]Zhang L, Li L, Cao Y, et al. *Catal. Sci. Technol.*, **2015**,**5**(4):2188-2196

[24]Yao X, Zhang L, Li L, et al. *Appl. Cata. B*: *Environ.*, **2014**, **150**:315-329

[25]Zhang D, Zhang L, Shi L, et al. *Nanoscale*, **2013**,**5**(3):1127-1136

[26]Aneggi E, Wiater D, de Leitenburg C, et al. *ACS Catal.*, **2014**,**4**(1):172-181

[27]Sayle T X T, Cantoni M, Bhatta U M, et al. *Chem. Mater.*, **2012**,**24**(10):1811-1821

[28]Sun C W, Sun J, Xiao G L, et al. *J. Phys. Chem. B*, **2006**, **110**(27):13445-13452

[29]Li C R, Sun Q T, Lu N P, et al. *J. Cryst. Growth*, **2012**,**343**(1):95-100

[30]Gong J, Meng F, Yang X, et al. *J. Alloys Compd.*, **2016**,**689**:606-616

[31]Yao X, Ma K, Zou W, et al. *Chin. J. Catal.*, **2017**,**38**(1):146-159